Available online at www.sciencedirect.com
ScienceDirect
Nuclear and Particle Physics Proceedings 273–275 (2016) 1134–1140

www.elsevier.com/locate/nppp

# ATLAS inner tracking detectors: Run 1 performance and developments for Run 2

Wolfgang Lukas, on behalf of the ATLAS Collaboration*

*University of Innsbruck, Institute for Astro- and Particle Physics, A-6020 Innsbruck, Austria*

**Abstract**

The measurement of charged-particle trajectories with the inner tracking detectors of the ATLAS experiment at the LHC is a key input for higher-level object reconstruction, ranging from leptons to the identification of heavy-flavor jets. The information provided by the inner tracking systems has also been proven to be very powerful for disentangling the effects of several interactions occurring in the same bunch crossing. In this contribution, the performance during the Run 1 data-taking period and preparation for the next run in 2015 is reviewed. In particular, it is shown how the passive material inside the inner tracking acceptance has been further studied in order to reduce the systematic errors on the tracking efficiency, with benefits for physics measurements. In addition, the developments in disentangling close-by tracks which naturally occur in the decay of very high-$p_{\mathrm{T}}$ objects (e.g. tau leptons) or jets are presented. The ongoing upgrade of the ATLAS detector includes an additional silicon layer (IBL) in the inner tracking system; the preparation for the integration of the new hardware and its expected performance is reviewed as well. Finally a summary of recent developments of the tracking software aiming for speed and disk-space optimizations is presented.

*Keywords:* ATLAS, detector performance, reconstruction, tracking, vertexing, alignment, clustering, pile-up

## 1. Introduction

Track and vertex finding are among the most challenging tasks in reconstructing $pp$, $pPb$ and $PbPb$ collision events recorded by the ATLAS detector [1]. Track finding requires the reconstruction of charged-particle trajectories from combinations of measurement points that are consistent with the hypothesis of trajectories. The precise measurement of charged-particle trajectories is fundamental to many physics analyses.

This report evaluates the performance of the inner tracking detectors of ATLAS during Run 1, which extended from the LHC startup in late 2009 until early 2013, and the developments for Run 2, which is scheduled to take place from early 2015 until late 2017 with higher luminosity and a larger expected average number of collisions per bunch-crossing (called *pile-up*).

Section 2 provides basic definitions and principles of charged-particle reconstruction in ATLAS. Studies of the detector material and its uncertainties are presented in Section 3. This is the dominant source of uncertainties of the track reconstruction efficiency, which is discussed in Section 4. Reconstructed tracks are used as an input for the vertex reconstruction, which is presented in Section 5, emphasising the challenge of high pile-up conditions. Reconstructed tracks from di-muon events are used for an alignment procedure which is described in Section 6. A novel neural network (NN) based pixel clustering algorithm, which improves tracking in dense environments, is presented in Section 7. Section 8 describes the upgrade of the ATLAS inner tracking system by installing an additional detector layer, as well as expected benefits on Run 2 tracking performance. New strategies and ongoing developments to constrain the CPU time for reconstruction under high pile-up conditions in Run 2 are addressed in Section 9. Finally all these studies are briefly summarised in Section 10.

*Email address: wolfgang.lukas@cern.ch

http://dx.doi.org/10.1016/j.nuclphysbps.2015.09.178

## 2. Charged Particle Reconstruction in ATLAS

The inner tracking system of ATLAS, called the Inner Detector (ID), consists of three main components: the Pixel detector, the Semiconductor Tracker (SCT), and the Transition Radiation Tracker (TRT). The Pixel and SCT detectors comprise silicon modules, while the TRT consists of drift tubes [1].

The ID track reconstruction consists of sequences of different algorithmic strategies [2], which use local and global pattern recognition algorithms to identify detector *measurements* or *hits* (clusters in the Pixel and SCT detector, drift circles in the TRT) that were produced by charged particles. By contrast, *holes* are defined as active detector modules where a measurement would be expected by a predicted charged-particle trajectory, but none was found nor assigned. A track fitting procedure is used to estimate the compatibility of measurements with the track hypothesis, thus forming track candidates. *Shared measurements* occur when a measurement is associated with several track candidates. Multiple track candidates for a single particle with almost identical measurements are partially removed by an ambiguity processor, which also suppresses *fake tracks* built from random measurement combinations. Remaining tracks are ranked based on the fit quality and assigned measurements and holes.

Tracks are used to reconstruct primary and secondary vertices. *Primary vertices* are found within the beam interaction region and provide information about the number and positions of the individual primary collisions. *Secondary vertices* are found outside the beam interaction region and are used to identify decays of heavy-flavour and long-lived particles.

The trajectories of tracks are parameterised using five track parameters as $\boldsymbol{\tau} = (d_0, z_0, \phi_0, \theta, q/p)$ [3]. The transverse momentum is given by $p_{\mathrm{T}} = p \sin\theta$ and the pseudorapidity $\eta$ is defined as $\eta = -\ln\tan(\theta/2)$.

The ID is designed to provide a transverse impact parameter resolution of approximately $\sigma_{d_0} = 140\,\mu\mathrm{m}/p_{\mathrm{T}}\,[\mathrm{GeV}] \oplus 10\,\mu\mathrm{m}$ and a longitudinal impact parameter resolution of $\sigma_{z_0\cdot\sin\theta} = 209\,\mu\mathrm{m}/p_{\mathrm{T}}\,[\mathrm{GeV}] \oplus 91\,\mu\mathrm{m}$ for reconstructed tracks [1]. Due to its proximity to the beam interaction region, the Pixel detector plays an important role in the estimation of the impact parameters.

The hit efficiencies of the main ID components during 2012 data taking were measured to be > 99% for the SCT, > 97% for the Pixel and > 94% for the TRT [4, 5]. The number of measurements-on-track and the distribution of reconstructed track parameters in 2012 data was well reproduced by Monte-Carlo (MC) simulation, giving confidence that the sensitive detector layers are correctly modelled in the simulation.

The accuracy of the reconstruction of charged-particle trajectories is limited by the combined effect of the finite resolutions of the detector elements, the knowledge of the locations of the detector elements, the knowledge of the magnetic field and the amount of material in the detector. The reconstruction is also affected by the occupancy of detector modules, particularly in dense environments resulting from jets.

## 3. Inner Detector Material Studies

An accurate detector geometry and material description in MC simulation is crucial for the assessment of track reconstruction inefficiencies and their systematic uncertainties due to particle-material interactions. Validation studies of the detector material were done using hadronic interaction vertices, photon conversions, and a tag-and-probe method to measure the SCT extension efficiency.

### 3.1. Hadronic Vertices

The location and amount of material in the ATLAS Inner Detector can be probed via reconstructed secondary vertices arising from hadronic interactions of primary particles. This was studied by comparing data from non-diffractive high-multiplicity $pp$ collisions at $\sqrt{s} = 7$ TeV and simulated events, using a minimum-bias trigger [6].

The reconstructed secondary vertices provide excellent spatial resolution ranging from $\sim 200\,\mu$m to 1 mm in both radial ($R$) and longitudinal ($z$) directions, depending on the radial distance of the secondary vertex from the collision point. This allows to study the precise location of the material and to compare it to the detector model.

The selection of track candidates coming from secondary vertices due to hadronic interactions is performed by requiring a large transverse impact parameter relative to the primary vertex of $d_0^{\mathrm{PV}} > 5$ mm, which removes > 99% of primary tracks and most tracks from $K^0_{\mathrm{S}}$ decays and $\gamma$ conversions, and by invariant mass vetoes on $\gamma$ conversion, $K^0_{\mathrm{S}}$ and $\Lambda$ candidates.

Figure 1 compares the radial data and MC distributions of the reconstructed secondary vertices. The beam-pipe at $R \approx 34$ mm as well as the three Pixel layers at $R \approx 50$, 88 and 122 mm are clearly visible, along with their service and support structures. Figure 2 shows the $(x, y)$ positions of the reconstructed secondary vertices in data and also reveals the beam-pipe shift of $r \approx 2$ mm with respect to the nominal (0,0) coordinate.

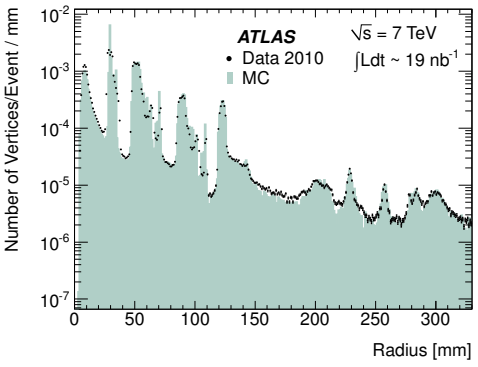


Figure 1: Radial positions of reconstructed secondary vertices from hadronic interactions for data (points) and MC (filled histogram), with $|z| < 300$ mm.

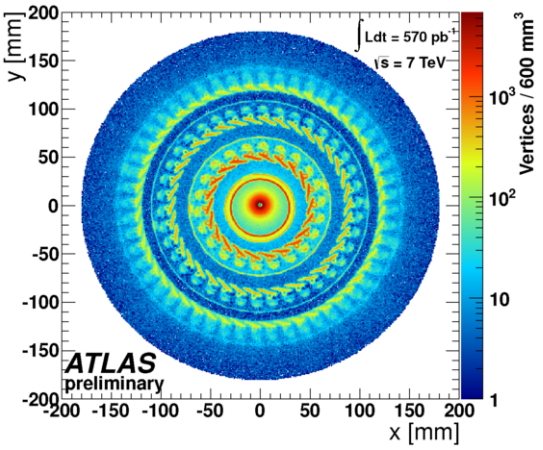


Figure 2: $(x, y)$ positions of reconstructed secondary vertices from hadronic interactions with $|z| < 300$ mm and $\sqrt{x^2 + y^2} < 180$ mm.

Using the same method, the complex structure of individual Pixel detector modules can be made visible. The observed discrepancies between data and MC, such as the mostly gaseous cooling fluid being described as liquid in the detector model, directly point to necessary improvements of the ATLAS detector model for MC simulations. These changes have now been incorporated.

With this technique, the overall material description in the simulation geometry is validated to within an experimental uncertainty of about 7% in the ID. Additional sources of systematic uncertainty include the modelling of hadronic interactions in MC simulation.

### 3.2. Photon Conversions

As the radiation length of a localised amount of material is related to the fraction of photons that convert within it, the converted photons can be used to map the material of the ID in front of the electromagnetic calorimeter [7].

Measurements inside the ID are compared to an accurately measured reference volume, for which the beampipe is chosen. In the course of these studies the description of ID support structures was improved, and good agreement in the distribution of photon conversions was found between data and MC simulation.

### 3.3. SCT Extension Efficiency

The SCT extension efficiency has been introduced as a technique to quantify the material located between the Pixel detector and the SCT using a standard tag-and-probe method. The principle of this technique is a measurement of the rate at which Pixel tracklets (track fragments reconstructed in the Pixel detector) are extended into the SCT by finding a combined track (tag) that matches the Pixel tracklet (probe). Track selection criteria are applied to the Pixel tracklets to ensure a high probe purity.

Hadronic interactions are the main source of tracklets for which the extension to combined tracks cannot be made. More traversed material leads to a higher probability for this type of particle-matter interaction, thus decreasing the extension efficiency. Therefore a good match in the SCT extension efficiency between data and MC corresponds to a proper description of the material budget in terms of nuclear interaction length.

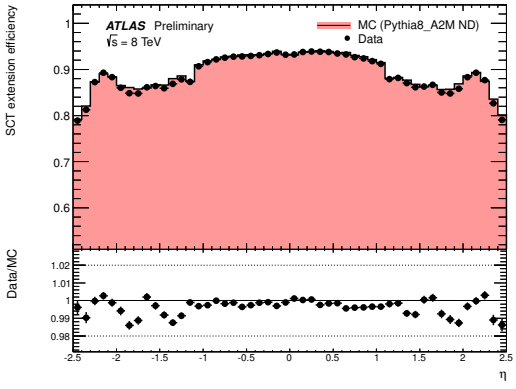


Figure 3: SCT extension efficiency as a function of $\eta$ of the pixel tracklets using ATLAS-GEO-21-01-00, which is equivalent to the final Run 1 geometry for results of this study.

Initial studies in 2012 revealed significant discrepancies between $\sqrt{s} = 8$ TeV data and MC simulation for

$2.2 < |\eta| < 2.5$ in the Patch Panel 0 (PP0) region, which is located within $174 < r < 218$ mm between the last sensitive Pixel layer and the first sensitive SCT layer, and which contains a significant amount of passive material from Pixel services. A detailed re-assessment of the Pixel services was performed via comparisons between the current ATLAS geometry model, original construction plans, and direct physical measurements of the ID in early 2013 during the LS1 (Long Shutdown 1) phase. These efforts converged in the final Run 1 geometry when no further improvements in the detector description could be found. The data/MC ratio of the SCT extension efficiency is visualised in Figure 3 as a function of the track parameter $\eta$.

The sensitivity of the SCT extension efficiency to additional material was assessed using dedicated simulation samples with distorted geometries. From comparisons to the nominal geometry, an overall uncertainty of $< 2\%$ was obtained for the passive material located between the Pixel and SCT detectors.

### *3.4. Summary*

By combining the results from ID material studies, for the final Run 1 detector geometry, the systematics due to material uncertainty can be described using a distorted geometry with +5% additional material in the whole ID.

## 4. Track Reconstruction Efficiency

The track reconstruction efficiency, $\varepsilon_{\text{trk}}$, is calculated and applied in various physics analyses in order to compensate for effects which affect the probability of a charged particle to be reconstructed. This factor is determined from MC and parameterised in bins of $p_{\text{T}}$ and $\eta$. It is defined as the ratio of reconstructed tracks matched to generated charged primary particles, $N_{\text{rec}}^{\text{matched}}$, to the number of all generated charged primary particles, $N_{\text{gen}}$:

$$\varepsilon_{\text{trk}}(p_{\text{T}}, \eta) = \frac{N_{\text{rec}}^{\text{matched}}(p_{\text{T}}, \eta)}{N_{\text{gen}}(p_{\text{T}}, \eta)},$$

where $p_{\text{T}}$ and $\eta$ are properties of the generated particle. The matching between a generated particle and a reconstructed track is done using a cone-matching algorithm in the $\eta$–$\phi$ plane. In addition, the particle trajectory must be compatible with the position of at least one pixel hit of the track.

The resulting $\eta$ distribution of the tracking efficiency for tracks with $p_{\text{T}} > 500$ MeV is shown in Figure 4. The shape of the $\eta$ distribution corresponds to the amount of ID material traversed by charged particles. The systematic uncertainties are dominated by the material uncertainty and were determined using a detector model with +10% additional material in the whole ID.

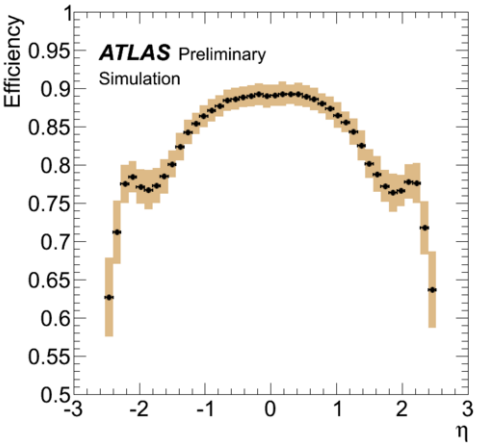


Figure 4: Track reconstruction efficiency as a function of $\eta$, obtained using the GEO-20 detector model, for tracks with $p_{\text{T}} > 500$ MeV. The systematic uncertainties were determined by comparison to a model with +10% additional material in the whole ID.

## 5. Vertex Reconstruction

The correct identification of the primary vertex from a hard-scattering process and the precise knowledge of the number of additional pile-up interactions is crucial for many physics analyses, especially at high pile-up conditions. Primary vertices are reconstructed from at least two tracks using an iterative vertex finding algorithm [8, 9].

During the Run 1 data taking periods of 2011 and 2012, mean numbers of 20 and 40 simultaneous $pp$ collisions (called *in-time pile-up* interactions) were reached in the ATLAS detector, respectively. The number of simultaneous $pp$ interactions per bunch crossing is distributed according to a Poisson distribution with a mean value of $\mu$ which typically decreases during a fill.

The correct identification of the hard-scatter primary vertex among all in-time pile-up vertices, which obscure hard-scatter physics signals, depends on the event multiplicity and the nature of the hard-scatter process.

A reconstructed vertex can either originate from a true single $pp$ interaction or fall into one of the following categories: (a) *fake vertices* are composed mostly of fake tracks, i.e. random combinations of detector measurements; (b) *split vertices* occur when a single $pp$ interaction is reconstructed as composed of several dis-

tinct vertices due to resolution effects, secondary interactions, etc.; (c) *merged* and *shadowed vertices* occur when several $pp$ interactions contribute to a single reconstructed vertex, or when the tracks produced in a hard-scatter $pp$ interaction are divided between close-by pile-up vertices or merged with one of them.

The effects of merging and shadowing are illustrated in Figure 5. This distribution is used to estimate the fraction of close-by vertices lost due to the shadowing effect, which becomes apparent in the region of small longitudinal separation $\Delta z$. The rate of merged vertices increases at higher pile-up. A reduction of this rate comes at the cost of an increase of split vertices, unless better algorithms can be applied.

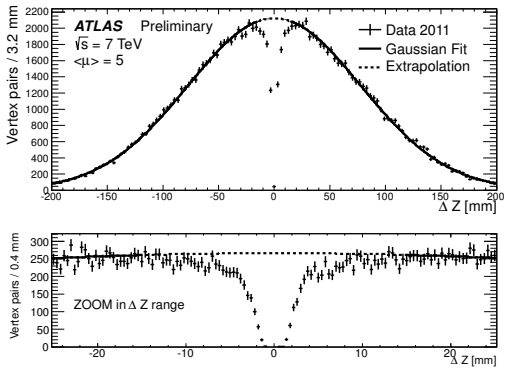


Figure 5: Longitudinal separation between primary vertices for minimum-bias events with two reconstructed primary vertices. The data were collected using a minimum-bias trigger in March-April 2011. The extrapolated Gaussian fit underlines the fraction of primary vertices missing due to merging of primary vertices at close distances.

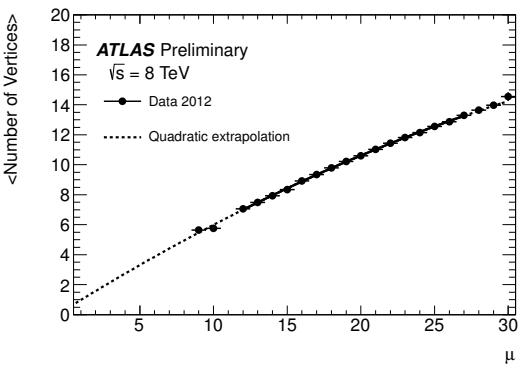


Figure 6: Average number of reconstructed primary vertices as a function of the average number of $pp$ interactions per bunch crossing $\mu$, measured for data collected in 2012 using the minimum-bias trigger.

The relation between the amount of in-time pile-up in each bunch crossing and the number of reconstructed primary vertices is affected by several processes, of which some are dependent on the true event multiplicity. The average number of reconstructed vertices in a minimum-bias sample is shown in Figure 6 as a function of the average number of interactions, measured with independent luminosity detectors, using the first data collected in 2012. The fake vertex contribution is controlled such as to be negligible even at high pile-up. This is achieved with tight quality selections of the input tracks used in the vertex reconstruction, thereby reducing the vertex reconstruction efficiency.

A fourth pixel layer, which has been installed during LS1 (see Section 8) at a smaller radial distance to the interaction point, will further improve the vertexing performance and vertex resolution during Run 2.

## 6. Detector Alignment

For precise physics measurements to be performed with the ID, the detector must be aligned to ensure that the positions of all the detector modules are precisely described. Failing to do so would degrade the resolution of tracks and potentially lead to biases in measured track parameters.

The alignment of the ID was performed using a track-based technique which minimises the track-to-hit residuals. Additional constraints, derived from $Z \to \mu^+\mu^-$ and $Z \to e^+e^-$ events, were introduced into the alignment to remove systematic biases from the geometry [10].

After successfully applying the procedure, the means of the distribution of residuals for each individual silicon module were obtained. It was found that the rms spread of these means was reduced to $< 1\,\mu$m. Systematic biases of the track parameters were determined to be less than $\delta d_0 < 1\,\mu$m ($\delta z_0 < 10\,\mu$m) for the transverse (longitudinal) impact parameters, while momentum biases are controlled to better than 0.1%. The accuracy of the alignment is highlighted by a measurement of the mass resolution of reconstructed $Z \to \mu^+\mu^-$ decays which shows a discrepancy of $< 1\%$ between data and MC.

## 7. Pixel Clustering

When a charged particle traverses a pixel sensor, charge is typically collected in more than one pixel. Groups of connected pixels, which are sharing at least one corner or edge with another pixel, are referred to as a *cluster*. The cluster information is used to estimate the track-module intersection position, taking into

account the incident angle and predicted incident position, including a correction for module distortions [10] (see Sec. 6). For primary charged particles with $p_{\mathrm{T}} >$ 400 MeV, cluster sizes reach up to 3 and 3.5 pixels in the transverse and longitudinal direction, respectively.

Clusters are identified by a connected component analysis (CCA). In dense environments, such as cores of highly energetic jets, a cluster can be made up from pixels traversed by multiple close-by particles, losing information about the number of traversing particles. In the worst case, one track candidate is completely disregarded to avoid the creation of duplicate tracks, which leads to an inefficiency in track finding.

A novel technique using a set of artificial neural networks (NN) has been developed [11] to identify and split merged clusters, in order to improve the double-track resolution (limit where two close-by tracks can still be reconstructed separately) and to reduce the number of shared measurements between tracks. The rate of falsely split clusters is kept below ~ 7.5%.

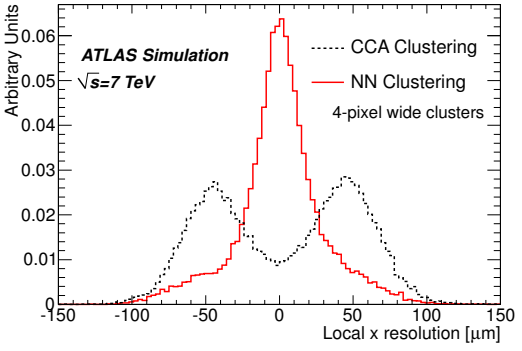


Figure 7: Cluster residual in the local $x$ direction for clusters with a width of four pixels reconstructed with the CCA clustering algorithm (dashed line) and the NN clustering algorithm (solid line).

Figure 7 shows the track-to-cluster residuals in the local $x$ direction for clusters with a transverse width of four pixels, comparing the NN clustering algorithm to the CCA algorithm. Most of these clusters stem from multiple particles or $\delta$-rays, which lead to a double peak structure in the CCA algorithm, reflecting the transverse pitch size of 50 $\mu$m. This double peak structure completely vanishes with the NN clustering algorithm. Remaining non-Gaussian tails originate from large-angle scattering, $\delta$-rays and clusters on the edges of modules, which typically have skewed distributions.

By improving the cluster position estimate, the NN clustering algorithm also enhances the impact parameter resolution with respect to the primary vertex by up to 7% (3%) in $z_0$ ($d_0$) compared to the CCA algorithm.

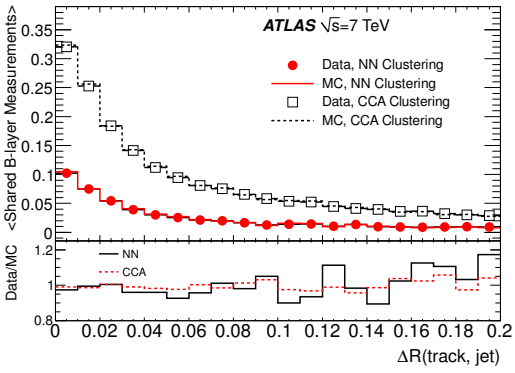


Figure 8: Average number of shared measurements in the B-layer on tracks associated to jets with 500 < $p_{\mathrm{T}}$ < 600 GeV for data and simulation, reconstructed with the CCA and NN clustering algorithms, as a function of the distance of the track from the jet center.

This effect has been studied on isolated tracks, using pairs of oppositely charged muons with $p_{\mathrm{T}} > 25$ GeV from $Z$ boson decay candidates.

Figure 8 shows that the NN clustering technique reduces the number of shared measurements at the innermost Pixel layer for tracks in highly energetic jets by up to a factor of three. The rate of shared measurements is accurately described by the MC simulation.

The NN clustering was introduced during the 2011 data-taking period and became the default approach for the rest of Run 1. Data taken earlier in 2011 were reprocessed to guarantee consistency for all Run 1 analyses. The new technique will be an essential component of the ATLAS track reconstruction in the upcoming Run 2, when the ID will be equipped with a new additional innermost silicon layer, as described in the next section.

## 8. Pixel Detector Upgrade (IBL)

The performance of the innermost Pixel detector layer (B-layer) is critical for the entire physics program of the ATLAS experiment. During the LS1 phase in 2013 and 2014, a fourth Pixel layer (Insertable B-Layer or IBL) was added to the Pixel detector between a new, smaller beam pipe and the previous innermost Pixel layer. This layer brings a number of benefits, such as increased tracking robustness against failure of pixel modules, higher b-tagging efficiency, and better vertexing performance and tracking precision due to the closer location to the interaction point.

Figure 9 shows the expected improvement in the transverse impact parameter resolution $\sigma_{d_0}$ due to the installed IBL. Similar results are obtained for other impact parameters except the transverse momentum which

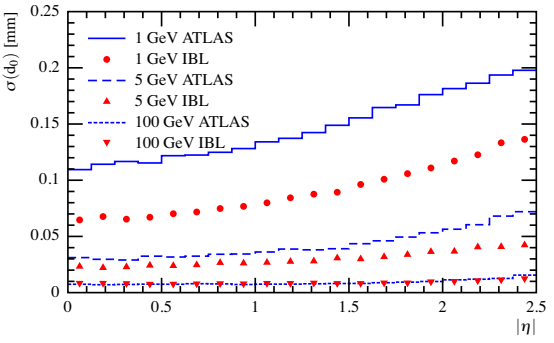


Figure 9: Expected transverse track parameter $d_0$ resolution for single muons at 1, 5 and 100 GeV as a function of $|\eta|$ for the ID without and with the IBL, obtained from simulation without pile-up.

remains unaffected. Furthermore, the improved vertex resolution due to the IBL increases the rate of reconstructed vertices under high pile-up conditions.

The IBL has been installed and commissioned in 2014 during LS1 and is ready for data taking in Run 2 from 2015 onwards.

## 9. Software Developments

As the track reconstruction from detector measurements is a combinatorial problem, the CPU time per reconstructed event increases non-linearly with higher pile-up. In order to cope with the pile-up conditions expected for Run 2 and the higher trigger event rate of 1 kHz, a number of optimisations were applied to the software framework.

These measures include a migration of the linear algebra library from CLHEP to Eigen, a compiler update and switch from GNU libm to the highly optimised Intel math library, updating the architecture from 32 to 64 bit, and an optimisation of the track-seeding strategies for high pile-up conditions.

The combination of these measures reduces the CPU time per reconstructed $t\bar{t}$ event with a pile-up of $\mu = 40$ by more than a factor of three, showing that the ATLAS reconstruction framework is well prepared for the high pile-up conditions in Run 2.

## 10. Conclusions

The performance of ATLAS inner tracking detectors in Run 1 was assessed by a number of studies including the material description, tracking and vertexing performance, and detector alignment. In addition a novel NN pixel clustering method was successfully introduced.

It was shown that the tracking and vertexing performance is under control even for the high pile-up conditions which are expected in Run 2. A new vertexing algorithm and the recently installed and commissioned fourth Pixel layer (IBL) further improve track parameter and vertex resolutions.

In summary, the ATLAS detector and reconstruction software framework are shown to be ready for Run 2 at the LHC which will begin in 2015.

**Acknowledgements:** This work was supported by the Austrian Federal Ministry of Science, Research and Economics (BMWFW).

## References

[1] ATLAS Collaboration, The ATLAS Experiment at the CERN Large Hadron Collider, JINST 3 (2008) S08003. doi:10.1088/1748-0221/3/08/S08003.
https://cds.cern.ch/record/1129811

[2] T. Cornelissen, et al., Concepts, Design and Implementation of the ATLAS New Tracking (NEWT), ATL-SOFT-PUB-2007-007.
https://cds.cern.ch/record/1020106

[3] F. Akesson, et al., ATLAS Tracking Event Data Model, ATL-SOFT-PUB-2006-004.
https://cds.cern.ch/record/973401

[4] ATLAS Collaboration, Operation and performance of the ATLAS semiconductor tracker. arXiv:1404.7473, doi:10.1088/1748-0221/9/08/P08009.
https://cds.cern.ch/record/1698966

[5] ATLAS Collaboration, Basic ATLAS TRT performance studies of Run 1, ATL-INDET-PUB-2014-001.
https://cds.cern.ch/record/1669603

[6] ATLAS Collaboration, A study of the material in the ATLAS inner detector using secondary hadronic interactions, JINST 7 (2012) P01013. arXiv:1110.6191, doi:10.1088/1748-0221/7/01/P01013.
https://cds.cern.ch/record/1394292

[7] K. Tackmann, ATLAS Inner Detector material studies. doi:10.3204/DESY-PROC-2010-01/195.
https://cds.cern.ch/record/1282090

[8] K. Grimm, et al., Methods to quantify the performance of the primary vertex reconstruction in the ATLAS experiment under high luminosity conditions, ATL-PHYS-PROC-2012-107.
https://cds.cern.ch/record/1457597

[9] ATLAS Collaboration, Performance of the ATLAS Inner Detector Track and Vertex Reconstruction in the High Pile-Up LHC Environment, ATLAS-CONF-2012-042.
https://cds.cern.ch/record/1435196

[10] ATLAS Collaboration, Alignment of the ATLAS Inner Detector and its Performance in 2012, ATLAS-CONF-2014-047.
https://cds.cern.ch/record/1741021

[11] ATLAS Collaboration, A neural network clustering algorithm for the ATLAS silicon pixel detector. arXiv:1406.7690.
https://cds.cern.ch/record/1712337

[12] ATLAS Collaboration, ATLAS Insertable B-Layer Technical Design Report, Tech. Rep. CERN-LHCC-2010-013. ATLAS-TDR-19, CERN, Geneva (Sep 2010).
https://cds.cern.ch/record/1291633